*Sensors & Transducers, Vol. 155, Issue 8, August 2013, pp. 86-97*

www.sensorsportal.com

**Sensors & Transducers**



*http://www.sensorsportal.com*

# Modeling and Simulation of Intra-Chip Wireless Propagation Channels for Hybrid WiNoC

**[1, 2] Jianhua Li, [1] Ning Wu, [2] Yongliang Hu**

[1] College of Electronic and Information Engineering, Nanjing University of Aeronautics and Astronautics, 210016, China;

[2] School of Mathematics & Information Engineering, Taizhou University, 317000 , China

[1] Tel.:+86 15868692009, fax: 057685137063

E-mail: ljh2007@tzc.edu.cn

*Received: 16 May 2013 /Accepted: 12 August 2013 /Published: 20 August 2013*

**Abstract:** The performance of traditional NoC architecture is limited in terms of throughput, delay and power consumption due to multi-hop wired links. The Wireless Network-on-Chip (WiNoC) has demonstrated their advantages as an emerging interconnect and communication architecture for the new-generation multi-core systems. In this work, we systematically analyze the propagation path of hybrid WiNoC under two on-chip antennas. Based on the deduction of reflection coefficient using 3-D Descartes coordinate system and the ray tracing, we model the intra-chip wireless propagation channel for hybrid Wyncote ensure the reliable communication, we evaluate the Bit-Error-Rate (BER) performance, delay spread and coherence bandwidth. Especially, the simulation based on the model shows that the Signal-Noise-Ratio budget at the end of receiver must be greater than 15 dB to ensure the BER performance for the on-chip wireless communication. It also demonstrates that the path loss for optical on-chip antenna could be improved about 6dB by elevating the height of antenna pairs. The channel coding scheme used for improving the system performance has been analyzed in detail. Besides, we propose an adaptive power control mechanism to maintain high performance by making a balance between BER, operating frequency and transmitted power.



**Keywords:** Wireless network-on-chip, Multi-path propagation, On-chip antenna, Path loss, Transmission coefficient.

## 1. Introduction

As the feature size of transistors is scaling down, chip designs are moving towards integrating a large number of IP cores onto a single die or System-on-Chips (SoCs) to satisfy the individual and multifunctional demands. The performance of SoCs will be limited by the ability to efficiently interconnect IP cores to accommodate their communication requirements. Due to the stringent power consumption limitation, the shared-bus has been shown to be unable to supply SoCs with both sufficient bandwidth and low latency. Network-on-Chip (NoC) has emerged as a promising interconnection architecture and communication platform for complex SoCs [1-2]. Although various topologies for NoC have been proposed to advance the design of the inter-core communication infrastructure [2], the data exchange between two distant blocks causes high latency and power consumption arising from multihop communication. According to the International Technology Roadmap

for Semiconductors (ITRS) in 2011, for the long term, metal material innovation with traditional scaling will no longer satisfy performance requirements of future designs and new interconnect innovations are needed [3].

Recently, several different emerging interconnect technologies have been considered to solve the performance limitation due to long range multi-hop wire line links. To provide ultralow latency and low power, the express virtual channels between selected nodes by inserting long range links in the a regular mesh networks is introduced in [4, 6]. It is shown that by using express virtual channels to connect distant cores in the network, it is possible to improve the NoC performance in terms of throughput, delay and power consumption. The performance of NoC is further improved by using global Lines for flow-control signals [5]. However, such solutions are difficult to alleviate the problems of skew, jitter and delay caused by long wired communication channel. Although these seem to be good methodologies that significantly improve performance when compared with a traditional wired NoC, it is not enough if the number of nodes increases to thousand or more. In addition, 3D integration using through silicon vias (TSVs) is adopted as a popular design methodology to reduce the latency and hops [7]. Despite their advantages, 3D NoC bring the new process challenges, such as finite thickness of IC, inter-layer contact patterning and low yield caused by vertical via failures. The heat dissipation caused by increased power density in 3D structure is also a serious problem. During to traditional wired interconnects based only on TDMA for data transmission, a new interconnect scheme named Radio Frequency Network-on-Chip (RFNoC) by using modern multiple access algorithms including CDMA, FDMA and microwave transmission line (MTL) to boost the bandwidth has been proposed [8, 9]. Although the channel has many benefits by inserting long on-chip multi-band MTL between distant blocks and also uses existing CMOS technology, it still require the long transmission lines to work as the wave guides. Optical interconnect NoC as a revolutionary approaches to improve performance in terms of bandwidth latency and power consumption [10, 11]. Despite optical interconnect has some advantages as a viable interconnect option, the optical modulators and detectors need much deeper investigation.

Wireless interconnect has been introduced to on-chip communication first in [12] for distributing clock signals. Then wireless interconnect has many advantages by comparing with other interconnects in [13]. Soon after a new on-chip communication system, dubbed Wireless Network-on-Chip (WiNoC) has been proposed in [14]. Since the achieved transmission range of UWB-based antenna is about 1 mm [15-17], which means in a chip whose area is 20 mm × 20 mm, this technology principally gives rise to multi-hop communication when transmitting data. Inspired by this wireless communication scheme, the chip multi-processors (CMPs) have more performance gains by using a scalable micro WiNoC interconnect structure [18]. In many cases, the additional latency of on-chip interconnects can have a significant impact on system performance. To further improve the performance of WiNoC, multi-hop wireless channels are replaced by inserting single-hop long-range wireless links [20-26]. Mass experiments show that WiNoC by using on chip antenna outperforms its more conventional wired counterpart [20, 21, 23], such as wired NoC, RFNoC, ONoC and so on. Thus it can be seen that WiNoC as a emerging interconnect solution has huge potential compared to traditional NoC to become the mainstream interconnect architecture and bridge the widening gap between computation requirements and communication efficiency for complex SoC system. The critical difference is the model of propagation channel between wired NoC and WiNoC.

However, aside from previous work in [25, 28], the model of wireless multi-path propagation channel for WiNoC have not been carefully investigated, despite its importance of intra-chip wireless interconnect. In order to more accurately simulate and evaluate the actual performance of system, the multi-path propagation channel is necessary to be explored and evaluated carefully for a given WiNoC. In this paper, we analyze on-chip antenna since it is the critical component for intra-chip wireless communication. A system-level model of wireless multi-path propagation channels for WiNoC is presented.

The remainder of the article is organized as follows: Section 2 presents two different on-chip antennas and their cross-sectional view. Section 3 presents the model of multi-path propagation channel for intra-chip wireless communication based on the reflection coefficient using 3-D Descartes coordinate system and ray tracing. The evaluation and simulation is reported in Section 4. Finally, Section 5 offers a brief set of conclusions and the future work.

## 2. On-Chip Antenna for WiNoC

The performance of intra-chip wireless interconnect is mainly dependent on antenna as the critical component for intra-chip wireless channel, thus we will ultimately need to incorporate antenna characteristics. Over the past few years, there considerable efforts have been done in terms of feasibility, measurement and signal propagation mechanisms of on-chip antenna for realizing the intra-chip wireless interconnect [27-34]. The on-chip antennas could be classified into two categories: millimeter-wave on-chip antenna operating at GHz frequency [30-32] and carbon nanotubes (CNTs) as optical on-chip antenna operating at THz frequency [33-34]. For the former, the transmission of radio signal is mainly realized with surface-wave rather than free-space wave through carrying out a large number of experiments and measurements [30, 31]. The simulated results show that the dominant

medium supporting the electromagnetic wave propagation is the silicon substrate [31]. For the latter, the carbon nanotubes (CNTs) as optical on-chip antenna operating at THz frequency transmit the optical signal at the true velocity of light through free-space [23, 33-34].

To make integration of on-chip antennas viably and obtain low-cost, it must be compatible with the substrate using mainstream silicon technologies. The cross-sectional views for integrated two different antenna pairs on silicon wafer with a dielectric layer inserted between the substrate and heat sink are shown in Fig. 1(a) [32] and Fig. 1(b).

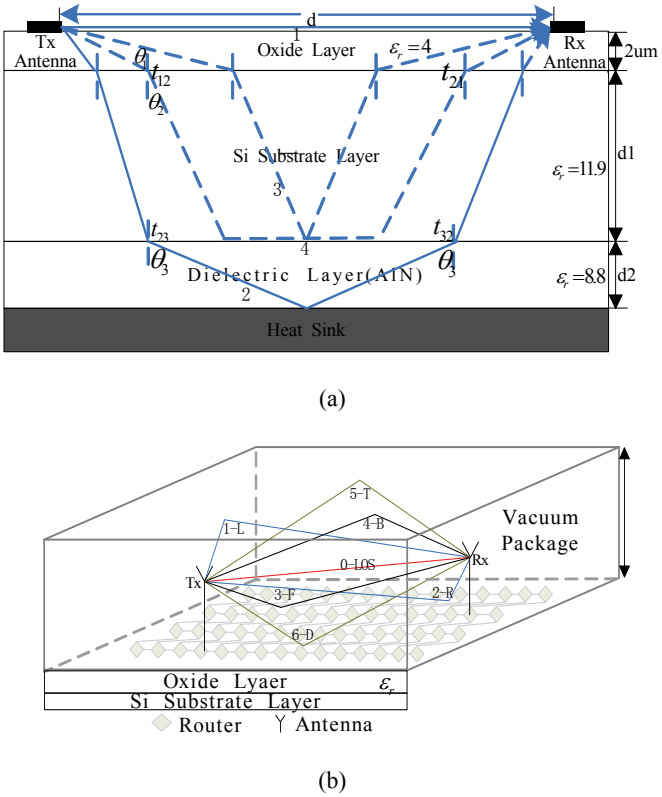


**Fig. 1.** Cross-Sectional View and Multi-Path Channel of WiNoC for Integrated Antennas on Silicon Wafer (a) Integrated Millimeter-Wave Antenna Pairs Operating at GHz, (b) Integrated Optical On-Chip Antenna Pairs Operating at THz.

## 3. Modeling of Multi-Path Propagation Channel

The wireless channel will be largely time invariant since there will be no motion for intra-chip transceivers. According to the classical theory of wireless communication system, the received signal is the sum of all the possible multi-path signal via a series of attenuation, time delay and phase shift. The typical mathematical model for multi-path channels is discrete multi-path time domain model. The multi-path channels could be seen as a linear band-pass filter. The shock response of multi-path channels is given by:

$$h(t) = \sum_{i=0}^{N-1} a_i e^{-j\varphi_i} \delta(t - \tau_i) \quad (1)$$

where i and N represent the i[th] path and the total number of multi-path, respectively; i=0 represents the first arrival path; $\tau_{RMS}$ is relative time delay to the first arrival path; $a_i$ and $\varphi_i$ represent the attenuation coefficient for amplitude and phase for the i[th] path at the time delay $\tau_{RMS}$.

The frequency domain transfer function for multi-path channels is given by:

$$H(f) = \int_{-\infty}^{+\infty} h(t) e^{-j2\pi ft} dt = \sum_{i=0}^{N-1} a_i e^{-j\varphi_i} e^{-j2\pi f \tau_i} \quad (2)$$

The received multi-path signals will produce time delay. The Root-Mean-Square Delay Spread (RMS-RDS) weighted proportional to the energy in the reflected paths is given by:

$$\tau_{RMS} = \sqrt{\sum_{i=0}^{N-1} p_i \tau_i^2 - (\sum_{i=0}^{N-1} p_i \tau_i)^2}, \quad (3)$$

where

$$p_i = \left| a_i \right|^2 \Big/ \sum_{i=0}^{N-1} \left| a_i \right|^2$$

The maximum data transfer rate depends on root-mean-squared delay spread $\tau_{RMS}$, which is the root-mean-square value of the delay of reflections, weighted proportional to the energy in the reflected waves. It will induce the frequency-selective fading and inter-symbol interference (ISI) if the data transfer rate is greater than the $1/\tau_{RMS}$.

### 3.1. Path Analysis of Multi-Path Propagation

To evaluate the impact on the performance of antenna integrated on a silicon wafer, here, we will carefully analyze the propagation path for two different on-chip antennas. To the millimeter-wave antenna pairs integrated on the oxide layer, the four possible paths for signal propagation as shown in Fig. 1(a). The path 1 represents the direct path between two antennas. It is called surface wave which may suffer attenuation due to the silicon substrate. The attenuation mainly depends on the distance between antennas, frequency and conductivity. Path 2 is the wave going through the dielectric layer and reflected back by the metal chuck. Among all these four paths, path 3 and path 4 are negligible because of the lossy silicon substrate. In this case, only path 1 and path 2 dominate [35]. The path which travel through the top oxide layer is neglected because the oxide thickness is negligibly small compared to a wavelength.

In Fig. 1(a), the electric field of surface wave in direct path 1 can be listed as [32]:

$$E_{sur} = E\frac{1}{d}e^{-\gamma_{sur}\cdot d} \tag{4}$$

where $\gamma_{sur} = \alpha + j\beta$ is the complex propagation constant of surface wave. $\alpha$ and $\beta$ represent the attenuation coefficient for amplitude and the propagation constant for phase shift. $d$ denotes antenna separation distance.

In path 2, the wave first goes into the silicon substrate, then into the insulating dielectric layer (e.g., AlN), and finally is reflected back by the heat sink to reach the receiving antenna. Similarly, the electric field formula of the wave in path 2 can be deduced as:

$$E_2 = \frac{E}{d}T_{12}T_{23}T_{32}T_{21}e^{[-\gamma_{si}\cdot 2d_1/\cos\theta_2]}e^{[-j\beta_{idl}\cdot 2d_2/\cos\theta_3 - j\pi]}, \tag{5}$$

where *d1* and *d2* represent the thickness of silicon substrate and thickness of insulating dielectric layer. $\gamma_{si}$ and $\beta_{idl}$ is complex propagation constant in silicon substrate and the propagation constant in insulating dielectric layer.$T_{12}$, $T_{23}$, $T_{32}$, and $T_{21}$ represent the transmission coefficients. The attenuation coefficient $\alpha$ and propagation constant $\beta$ are defined as follows:

$$\alpha = \omega\sqrt{\frac{\mu\varepsilon}{2}}\left[\sqrt{1+\left(\frac{\sigma}{\omega\varepsilon}\right)^2}-1\right]^{\frac{1}{2}} \tag{6}$$

$$\beta = \omega\sqrt{\frac{\mu\varepsilon}{2}}\left[\sqrt{1+\left(\frac{\sigma}{\omega\varepsilon}\right)^2}+1\right]^{\frac{1}{2}} \tag{7}$$

According to above analysis, the total electric field of the wave for millimeter-wave antenna pairs operating at GHz frequency is given by

$$E_{G\text{-}total} = E_{sur} + E_2 \tag{8}$$

However, as shown in Fig. 1(b), there are seven different paths to CNTs as the optical on-chip antenna in free-space. It has become a viable candidate to create a vacuum for line of sight (LOS) communication operating at THz/optical frequency by elevating the chip packaging material from the substrate. From the electric field, the total electric field intensity as a function of transmission distance could be expressed by:

$$E_{T\text{-}total} = \frac{E_d}{d}e^{-\gamma d} + \sum_{i=1}^{6}\frac{E_i}{L_i}R_{0i}e^{-rL_i} \tag{9}$$

where $E_d$ is the electric field intensity of LOS communication. *i* represents the $i^{th}$ surface of all six surfaces(i.e., Left, Right, Front, Back, Top or Down surface corresponding to the path 1-L, 2-R, 3-F, 4-B, 5-T, 6-D in Fig. 1(b), respectively) of the chip packaging. The *d* is the LOS distance between a transmitting antenna and a receiving antenna. $L_i$ is the reflection path length traveled by the wave through the $i^{th}$ surface.$R_{0i}$ is the reflection coefficient while ray travel from free-space to the $i^{th}$ surface of packaging material. In free-space, where the attenuation constant $\alpha$ =0, so the complex propagation constant $\gamma = \alpha + j\beta = j\beta$.

### 3.2. Reflection and Transmission Coefficient based on 3-D Descartes Coordinate System

Though there is no moving for the intra-chip communication, the multipath propagation will be induced by the reflections of dielectric surfaces. According to wireless communication system theory, the received signal could be deduced by reflection and transmission coefficient based on ray tracing. The simplified two ray reflection model as shown in Fig. 2.

Since the angle of incidence $\theta_1$ is difficult to obtain in reality, 3-Dimension descartes coordinate system has been adopted to express the reflection

coefficient. We suppose that the value of descartes coordinate for $T_x$ antenna and $R_x$ antenna are ($x_t$, $y_t$, $z_t$) and ($x_r$, $y_r$, $z_r$), respectively. Here, $z_t$ and $z_r$ could be seen as the heights of transmitting and receiving antenna. H is the height of vacuum packaging above the oxide layer.

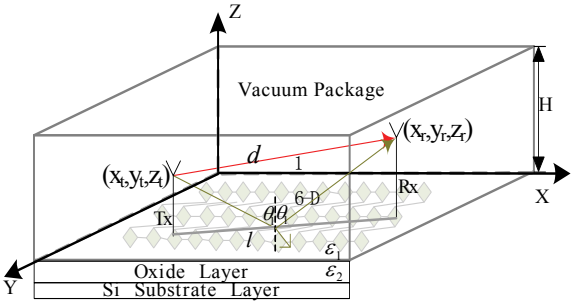


**Fig. 2.** Two Ray Reflection Model for WiNoC.

The $l$ is the projection of the direct LOS length $d$ on the X-Y plane. The direct LOS length d can be expressed by

$$d = \sqrt{l^2 + (z_r - z_t)^2}\,, \tag{10}$$

where $l = \sqrt{(x_r - x_t)^2 + (y_r - y_t)^2}$, the relationship between distance $l$ and angle of incidence θ could be expressed by

$$l = (z_r + z_t)tg\theta \tag{11}$$

The reflection coefficient $R_{06}$ (i.e., the path 6-D traveled from free-space to down-surface) and transmission coefficient $T_{12}$ usually depend on the permittivity $\varepsilon$ of the surface materials, the angle of incidence $\theta_1$ and polarization mode, are defined as [36]:

$$R_{06//} = \frac{\cos\theta_1 - \sqrt{\frac{\varepsilon_2}{\varepsilon_1} - \sin^2\theta_1}}{\cos\theta_1 + \sqrt{\frac{\varepsilon_2}{\varepsilon_1} - \sin^2\theta_1}} \tag{12}$$

$$R_{06\perp} = \frac{\frac{\varepsilon_2}{\varepsilon_1}\cos\theta_1 - \sqrt{\frac{\varepsilon_2}{\varepsilon_1} - \sin^2\theta_1}}{\frac{\varepsilon_2}{\varepsilon_1}\cos\theta_1 + \sqrt{\frac{\varepsilon_2}{\varepsilon_1} - \sin^2\theta_1}} \tag{13}$$

where $R_{06//}$ or $R_{06\perp}$ is reflection coefficient at down surface for the horizontal or vertical polarization, respectively. The transmission coefficient for the horizontal or vertical polarization could be computed according to the eqs. (12) and (13).

$$1 + R_{//(\perp)} = T_{//(\perp)} \tag{14}$$

According to the above deduce, so the length of path 6-D could be expressed as:

$$L_6 = \sqrt{l^2 + (z_r + z_t)^2} \tag{15}$$

Combining eqs. (11)-(13), the reflection coefficient formula using 3-Dimension Descartes coordinate system can be deduced as follows:

$$R_{06//} = \frac{(z_r + z_t) - \sqrt{(\frac{\varepsilon_2}{\varepsilon_1} - 1)l^2 + \frac{\varepsilon_2}{\varepsilon_1}(z_r + z_t)^2}}{(z_r + z_t) + \sqrt{(\frac{\varepsilon_2}{\varepsilon_1} - 1)l^2 + \frac{\varepsilon_2}{\varepsilon_1}(z_r + z_t)^2}} \tag{16}$$

$$R_{06\perp} = \frac{\frac{\varepsilon_2}{\varepsilon_1}(z_r + z_t) - \sqrt{(\frac{\varepsilon_2}{\varepsilon_1} - 1)l^2 + \frac{\varepsilon_2}{\varepsilon_1}(z_r + z_t)^2}}{\frac{\varepsilon_2}{\varepsilon_1}(z_r + z_t) + \sqrt{(\frac{\varepsilon_2}{\varepsilon_1} - 1)l^2 + \frac{\varepsilon_2}{\varepsilon_1}(z_r + z_t)^2}} \tag{17}$$

The other reflection coefficients (e.g., $R_{01}$~$R_{05}$) and path length (e.g., L1~L5) could be computed as above.

### 3.3. Path Loss Model for Wireless Propagation Channel

In classical antenna theory, the power is directly proportional to the square of the electric field intensity. The figure of merit for an on-chip antenna pair is the power transmission gain between a receiving ($P_R$) and a transmitting antenna ($P_T$).It is represented using Friis transmission formula [33] and shown in (18):

$$\frac{P_R}{P_T} = |S_{21}|^2 = (1 - |\Gamma_t|^2)(1 - |\Gamma_r|^2)G_t G_r (\frac{\lambda}{4\pi d})^2 e^{-2\alpha R} \tag{18}$$

where $\Gamma_t$ or $\Gamma_r$ is the reflection coefficient for the transmitting or receiving antenna, respectively. $G_t$ and $G_r$ are the transmitting and receiving antenna gain. λ and $d$ represent the wavelength based on the effective dielectric constant $\varepsilon_r$ and the antenna separation distance. α is the attenuation constant. In free-space, where the attenuation constant α=0. $S_{21}$ is the transmission coefficient.

The path loss for wireless multi-path propagation is calculated from ray tracing model. To GHz millimeter-wave antenna pairs, the two-ray path loss $PL_G$ combining eqs. (4), (5) and (8) is given by

$$PL_G = (4\pi)^2 \Bigg/ \left| \frac{\lambda_{sur} \cdot G_d \cdot e^{-\gamma_{sur} d}}{d} + T \frac{\lambda_{si} G_2 \cdot e^{[-\gamma_{si} \cdot 2d_1/\cos\theta_2]} e^{[-j\beta_{dll} \cdot (2d_2/\cos\theta_3) - j\pi]}}{d'} \right|^2, \tag{19}$$

where $\lambda_{sur}$ and $\lambda_{si}$ are the wavelength of surface wave and silicon substrate, respectively. T is the products of transmission coefficient for each layer.

For the same theory , the path loss $PL_T$ combining the eqs. (6), (7) and (9) to the THz optical on-chip antenna pairs in free-space is given by:

$$PL_T = \left(\frac{4\pi}{\lambda}\right)^2 \Bigg/ \left| \frac{G_{t0}G_{r0}e^{-j2\pi d/\lambda}}{d} + \sum_{i=1}^{6} R_{0i} \frac{G_{ti}G_{ri}e^{-j2\pi L_i/\lambda}}{L_i} \right|^2, \quad (20)$$

where $\lambda$ is the wavelength in free-space. According to eqs. (15)-(17), $R_{0i}$ and $L_i$ could be computed based on 3-D descartes coordinate system and ray tracing. $G_{ti}$ and $G_{ri}$ is the transmitting antenna and receiving antenna field radiation pattern functions for the $i^{th}$ path.

### 3.4. Delay Spread and Coherence Bandwidth

The Doppler spread effects arise from the multi-path propagation are negligible since the fixed position of transmitting and receiving antenna for intra-chip wireless communication, however the delay spread is a very important parameter must taken into consideration for multi-path channel. No serious ISI is likely to occur if the symbol duration is longer than the RMS delay spread. The coherence bandwidth $B_c$ as another important channel parameter is given by

$$B_c \approx \frac{1}{\tau_{RMS}} \quad (21)$$

The receiver will not identify the symbol correctly as propagation channel producing serious signal distortion and high BER if the symbol rate is bigger than the coherence bandwidth $B_c$. Channel coding mechanism and equalization technology are needed to solve the ISI if the maximum symbol rate $R_s$ is bigger than the coherence bandwidth $B_c$. However, these measures are beyond the scope of this paper. The $B_c$ is easy to obtain according to eqs. (3) and (21) for two different on-chip antenna pairs. The maximum symbol rate $R_s$ is less than $B_c$.

### 3.5. SNR and BER Performance of WiNoC

The performance for hybrid WiNoC system depends on the signal-to-noise ratio (SNR) and BER. It is found that the signal is distorted by the thermal noise and switching noise within the packaging [28]. The SNR for the receiver is defined as

$$SNR = \frac{E_{rb}}{N_0 + S_0}, \quad (22)$$

where $N_0$ and $S_0$ represent the power spectral density of thermal noise and switching noise. However, the wireless channels are in very high frequency band and the switching noise coupled to the antenna is common-mode, thus the intra-chip switching noise power spectral density to the WiNoC is negligible.

In equation (22), the average energy per bit at receiving end, $E_{rg}$ , is calculated as [28]:

$$E_{rb} = E_{tb} + G_{tr} + G_r, \quad (23)$$

where $E_{tb}$ is the transmitted energy per bit, $G_{tr}$ is the average value of the transmission gain between the transmitting and receiving antennas, and $G_r$ is the gain of the receiver.

The thermal noise power spectral density, $N_0$ , is calculated as

$$N_0 = K T_0 F = K T_0 \left(\frac{T_{antenna}}{T_0} + F_r\right), \quad (24)$$

where $K$ is the Boltzmann constant, $T_0$ is the room temperature taken as 290 K typically, $T_{antenna}$ is the temperature of antenna assumed to be 330 K, and $F_r$ is the receiver noise figure (taken as 4 dB generally). This assumption is supported by a recent study of CMOS integrated circuit.

The wireless channels for WiNoC have different bit-error rate function at different modulation mode (e.g., OOK, BFSK, BPSK). The on-off keying (OOK) and binary phase-shift keying (BPSK) are usually adopted with respect to wireless channels for WiNoC [21, 25-26].

To simulate a WiNoC system, some necessary changes should be made since there are differences between the WiNoC and NoC architectures, such as the channel's character, number of nodes, combination of protocols (intra- and inter- subnet) used in the system and routing algorithms. Still, there is no general simulator for WiNoC for public use.

Establishment of accurate wireless channel model has important guidance values for dynamic power management of wireless link, obtaining low bit-error rate, overcoming inter-channel interference (ICI) and ISI.

## 4. Simulation Results and Discussion of Wireless Multi-Path Channel Model

In this section, we simulate and analyze the characteristics of the proposed on-chip wireless channel model, including reflection coefficient versus distance, path loss as a function of operating frequency or distance, and the comparison of BER under different coding. The BER performance has been greatly improved by making a trade-off between operation frequency and transmitted power.

### 4.1. Reflection Coefficient Versus Antenna Separation Distance

According to eqs. (10)-(17), it can be seen that the reflection coefficients depend upon the dielectric

constant $\varepsilon_r$ and the optical antenna separation distance $d$. The simulation results are illustrated in Fig. 3(a) and 3(b).From the Fig. 3(a), we can observe that the value of $R_{//}$ is negative and decrease significantly with distance, and also the $R_{\perp}$ pass through the zero and decrease with the distance at different value of $\varepsilon_r$. The $R_{\perp}$ tends to be negative only when separation distance is large enough, e.g., 4-7 mm.

Since the current in vertical polarization way is less than that in horizontal polarization way, the vertical polarization is adopted to reduce propagation attenuation induced by the dielectric surfaces in this experiment. Fig. 3(b) shows that the variation of the reflection coefficient over the 20 mm × 20 mm die area using vertical polarization. It's evident that the value of $R_{\perp}$ increases with the $\varepsilon_r=\varepsilon_2/\varepsilon_1$ and decreases with the optical antenna separation distance.

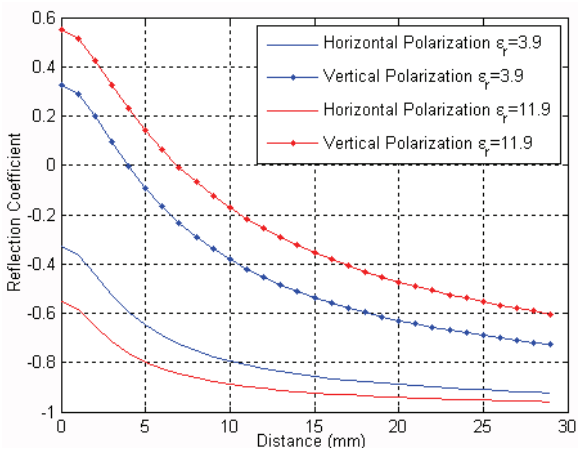


(a)

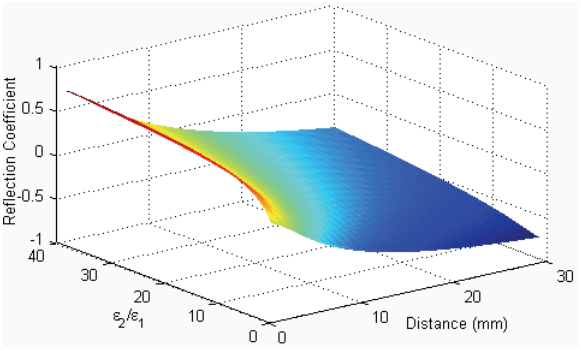


(b)

**Fig. 3.** Simulated (a)Horizontal polarization and Vertical polarization versus distance $d$, and (b)Vertical polarization versus distance and $\varepsilon_r=\varepsilon_2/\varepsilon_1$.

## 4.2. Path Loss Versus Distance, Antenna Height and Frequency

Fig. 1(a) shows that the oxide layer of thickness 2 μm was grown on the silicon substrate and a dielectric layer was used at GHz frequency to improve isolation and attenuation. The path loss for wireless propagation channel as a function of separation distance between antennas has already been shown in Fig. 4 according to eqs. (19) and (20). Fig. 4(a) and 4(b) show that the path loss increase obviously with separation for both millimeter-wave on-chip antenna and CNTs as optical on-chip antenna. It's found that the path loss could be reduced about 12 dB on average by increasing the resistivity of silicon substrate from 2 Ω-cm to 5 kΩ-cm.

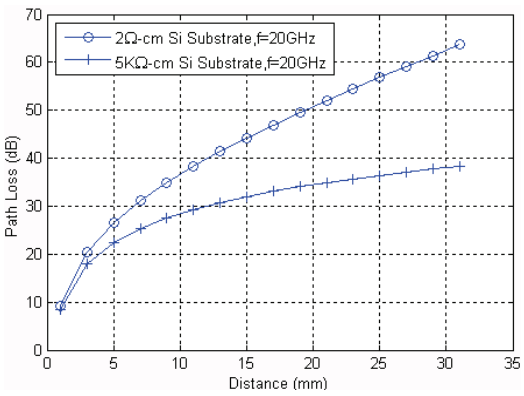


(a)

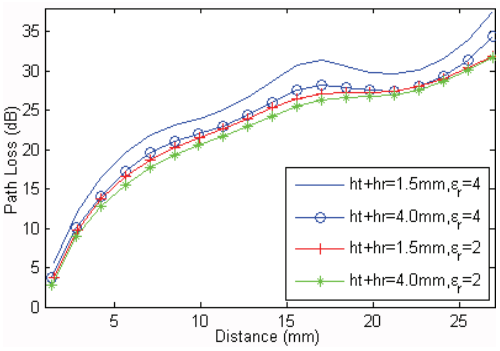


(b)

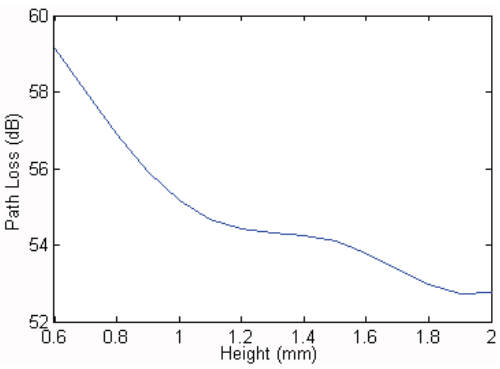


(c)

**Fig. 4.** (a) Path loss versus distance for different silicon substrate resistance at GHz frequency; (b) Path Loss versus distance and height of optical on-chip antenna operating at THz frequency; (c) Path loss versus sum of height of transmitting and receiving antenna pairs.

As illustrate in Fig. 4 (b), the path loss of on-chip optical antenna varies with dielectric constant and the sum of the height of transmitting and receiving antenna pairs. It's feasible to improve the path loss about 6-10 dB on average by increasing the height of antenna pairs and using low-loss dielectric layer .

Moreover, from Fig. 4 (c) it can be observed that the path loss in THz frequency range could be improved about 6 dB by elevating the height of antenna pairs from 0.6 mm to 2 mm. But this improvement is achieved at the cost of area overhead.

Besides those, the path loss as a function of frequency for two types of on-chip antennas, biased on full electromagnetic-wave simulation software, Ansoft HFSS, are illustrated in Fig. 5. High resistivity silicon substrate ($\rho$ = 5 k$\Omega$-cm) is used for the simulation of wireless channel. As can be seen, the path loss doesn't always increase with the frequency for the millimeter-wave antenna. From the simulation results in Fig. 5 (a) it is observed that the gain is high in the window's region. It suggests that the operating frequency of on-chip wireless communication should be allocated within the high gain window for achieving better performance. Furthermore, it is found that the transmission gain decreases with distance especially in window's region and increases obviously with the frequency range of 10-28 GHz.

As can be seen from Fig. 5 (b), the path loss in THz frequency range versus distance goes through ups and downs and has many minimax values as a result of the interaction between in-phase and anti-phase of reflection paths. It also demonstrates that the path loss doesn't present window's region because the THz operating frequency is far beyond the resonant frequency of antenna.

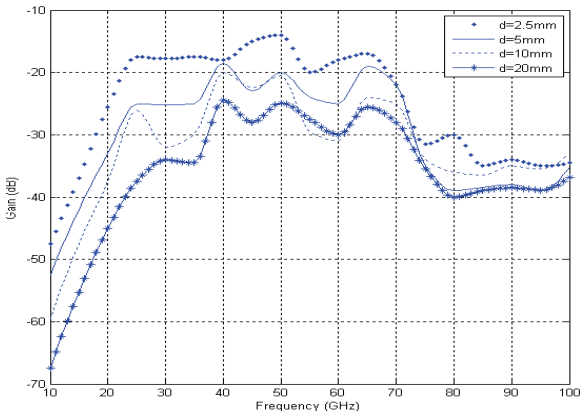


(a)

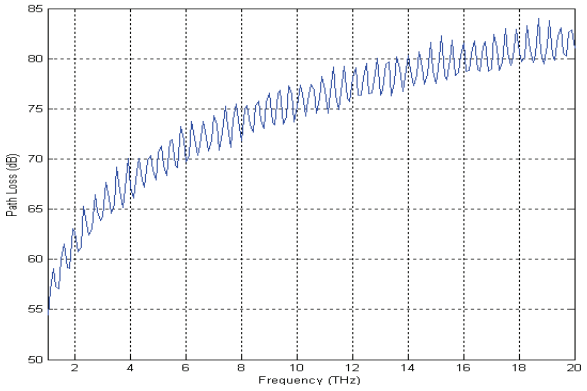


(b)

**Fig. 5.** (a) Gain versus frequency for different separation distance at GHz frequency (b) Path Loss versus frequency operating at THz.

## 4.3. RMS-RDS and Coherence Bandwidth

Apart from path loss, delay spread is another important factor for an on-chip wireless propagation channel. In an on-chip wireless communication system with high bit rate, the reliability and efficiency will be reduced as frequency-selective fading and ISI. As can be seen from Fig. 6, the $\tau_{RMS}$ and coherence bandwidth $B_c$ for optical antenna using vertical polarization as a function of distance don't always increase or decrease with symmetric distance.

It's apparent that while distance is approximately equal to 10.8 mm, the maximum of the $\tau_{RMS}$ is about 3.03 ps, and also the $B_c$ shows the minimum under the maximum of $\tau_{RMS}$. Moreover, the $\tau_{RMS}$ for WiNoC using optical antenna is less than that for WiNoC using millimeter-wave antenna [29]. Furthermore, it proved that the signal propagation through free-space for optical on-chip antenna is fast than that through silicon-substrate for millimeter-wave antenna.

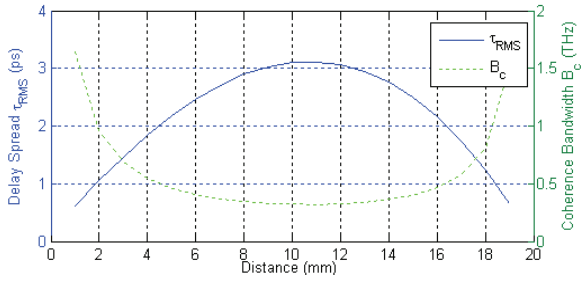


**Fig. 6.** Delay spread and $B_c$ versus separation distance for optical antenna using vertical polarization.

## 4.4. Simulation and Discussion of SNR and BER

To further estimate the characteristics of the proposed on-chip wireless channel model, the BER performance is must be considered. The BER of the wireless communication for WiNoC is totally determined by the SNR of the receiver. Especially, the coding scheme and SNR must be analyzed to ensure the quality of service QoS for supporting low BER communication.

The simulation based on Simulink software was carried out to estimate the BER performance. Fig. 7 shows the block diagram of on-chip wireless communication system. The modulated data go through both AWGN and Wireless Multi-Path Channel. In our simulation, we assumed that the output power Pt is set to be -15 dBm for the transmitter, and the thermal noise of substrate is set to be 174 dBm/Hz. Thus, the SNR at the end of receiver can be calculated as:

$$SNR_t = P_t\text{-PathLoss-}(-174)\text{-NF-}10\log B \quad (25)$$

where NF is the noise figure of the receiver including LNA and Mixer. B is the bandwidth.

The required SNR was adopted for the targeted BER of $10^{-14}$, which is the BER of traditional RC wires [18]. Fig. 8 (a) illustrates the BER performance of on-chip wireless modulation/demodulation system with different coding methods and without coding, while silicon substrate resistance is equal to 5 kΩ-cm. As shown in Fig. 8, it's evident that the RS or Hamming coding scheme improve the BER performance, especially when the SNR is greater than 5 dB or the separation distance is less than 20 mm. From the point of communication distance, it suggests that it's very suitable for the hybrid WiNoC by inserting long-range wireless links in place of multi-hop wire line links. So, it becomes essential to apply channel coding scheme as simple as possible for improving the BER performance of WiNoC.

As illustrated in Fig. 9, we can observe that the BER performance will be improved significantly by increasing the operating frequency from 10 to 20 GHz. Again, simulation in Fig. 9 indicates that channel coding scheme offers a great advantage in term of BER performance improvement especially when the SNR value at the receiver is higher than 5 dB.

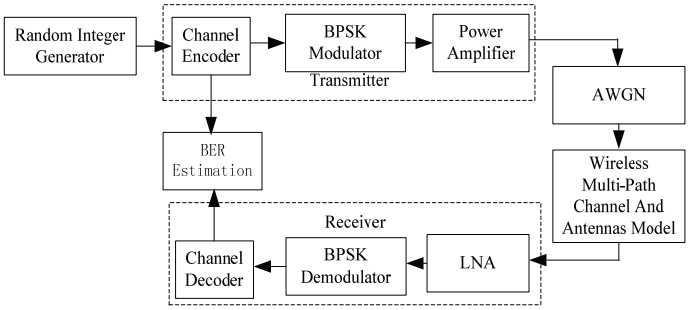


**Fig. 7.** Simulation block diagram for wireless modulation/demodulation system.

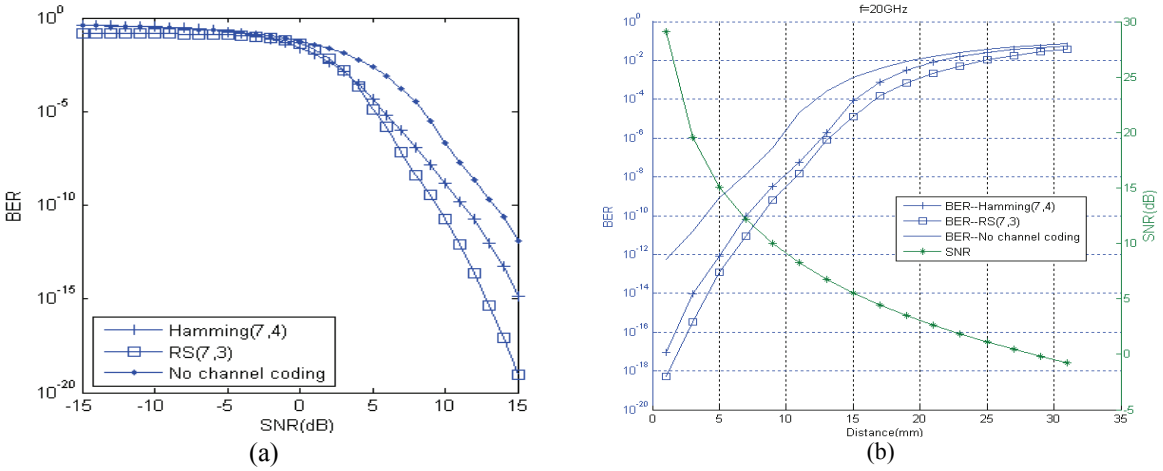


**Fig. 8.** In GHz frequency range (a) BER performance versus SNR, (b) BER performance and SNR versus separation distance.

## 4.5. A Trade-off between BER, Operating Frequency and Transmitted Power

As can be seen from Fig. 8(b), although the maximum communication distance of hybrid WiNoC is less than 28 mm, the BER of the WiNoC is less than $10^{-3}$ at $P_t$=-15 dBm, which is not enough for hybrid WiNoC. This value of BER is far higher than that of traditional wired links (about $10^{-14}$). To maintain the same low BER as wired NoC, from Fig. 8(a) we can observe that the $SNR_t$ budget at the end of receiver must be greater than the minimum $SNR_{min}$ (about 15 dB).

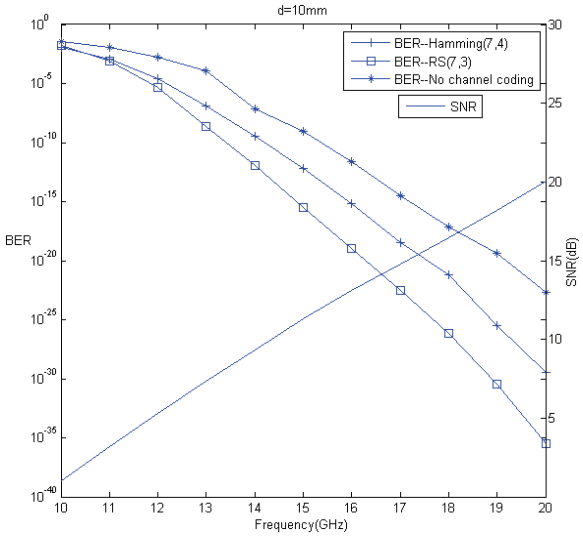


**Fig. 9.** BER performance as a function of GHz operating frequency at a distance of 10 mm.

Traditionally, in order to ensure enough power and BER performance for all the transmissions, the worst-case power loss in the WiNoC is considered, and the $P_t$ is set to a fixed value offering the worst-case power for the all communication. Thus, it will causes the changes of SNR within a large dynamic rang for receiver. This will produce unnecessary power consumption for some data traffic. As shown in Fig. 8 and Fig. 9, we could make a direct tradeoff between BER, operating frequency and transmitted power to realize adaptive power control. Depending on the separation distance, it is possible to consume more or less power and bandwidth to compensate for the BER. In other words, for a short distance communication ranging from 0 mm to 5 mm with high SNR, the transmitter will maintain a low $P_t$ and operating frequency. Likewise, for a a medium-distance ranging from 5 mm to 15 mm, only the operating frequency will be increased. For a long distance that is greater than 15 mm, both operating frequency and $P_t$ will be enhanced to ensure the lower power consumption and BER performance.

## 5. Conclusions and Future Work

In this paper we systematically analyzed the propagation path of hybrid WiNoC under two on-chip antennas, including millimeter-wave on-chip antenna operating at GHz frequency and optical on-chip antenna operating at THz frequency. Base on those analyses, we modeled the wireless multi-path propagation channel for hybrid WiNoC. Especially, the path loss model has been present based on reflection coefficient using 3-D Descartes coordinate system for optical on-chip antenna. To ensure the reliable communication, the BER performance, delay spread and coherence bandwidth have been evaluated in detail. The simulation results demonstrate that the path loss could be reduced about 12 dB on average by increasing the resistivity of silicon substrate. It also shows that the path loss in THz frequency range could be improved about 6 dB by elevating the height of antenna pairs from 0.6 mm to 2 mm. Especially to improve the BER performance, we proposed a channel coding scheme to realize error control. Furthermore, through analyzing the influence factors of BER, the simulation based on the model shows that the SNR budget at the end of receiver must be greater than 15 dB. In order to ensure the overall performance for the on-chip wireless communication. We proposed an adaptive power control mechanism by making a balance between BER, operating frequency and transmitted power.

In ongoing and future investigations, we intend to evaluate the area and power consumption overhead under different coding scheme for improving the BER performance. Furthermore, we will improve the coding with no handshaking communication to reduce the communication delay and power.

## Acknowledgements

This work is supported by the National Natural Science Foundation of China under Grant No. 61076019 and the Natural Science Foundation of Zhejang Province of China under Grant No. LY13F020012.

## References

[1]. L. Benini, G. D. Micheli, Networks on Chips: A New SoC Paradigm., *Computer*, Vol. 35, No. 1, January 2002, pp. 70-78.

[2]. Reza Sabbaghi-Nadooshan, Mehdi Modarressi, Hamid Sarbazi-Azad, The 2D SEM: A novel high-performance and low-power mesh-based topology for networks-on-chip, *International Journal of Parallel, Emergent and Distributed Systems*, July 2010, pp. 331–344.

[3]. ITRS, http://www.itrs.net/Links/2011ITRS/Home2011.htm

[4]. A. Kumar et al., Toward Ideal On-Chip Communication Using Express Virtual Channels, *IEEE Micro.,* Vol. 28, No. 1, February, 2008, pp. 80-90.

[5]. T. Krishna et al., NoC with Near-Ideal Express Virtual Channels Using Global Line Communication, in *Proceedings of the IEEE Symposium on High Performance Interconnects (HOTI),* August 2008, pp. 11-20.

[6]. U. Y. Orgras, R. Marculescu, Its a Small World After All: NoC Performance Optimization via Long-Range Link Insertion, *IEEE Transactions Very Large Scale Integration (VLSI) Systems,* Vol. 14, No. 7, July 2006, pp. 693-706.

[7]. Brett Stanley Feero, P. Pande, Networks-on-Chip in a Three-Dimensional Environment: A Performance Evaluation, *IEEE Transactions on Computers*, Vol. 58, No. 1, January 2009, pp. 32-45.

[8]. Mau-Chung Frank Chang, Ingrid Verbauwhede, Charless Chien et al, Advanced RF/Baseband Interconnect Schemes for Inter- and Intra-ULSI

Communications, *IEEE Transactions on Electron Devices,* Vol. 52, No. 7, July 2005, pp. 1271-1285.

[9]. M. Frank Chang, Jason Cong, Adam Kaplan, et al., CMP network-on-chip overlaid with multi-band RF-interconnect, in *Proceedings of the IEEE 14th International Symposium on High Performance Computer Architecture (HPCA-14),* February 2008, pp. 191-202.

[10]. J. Zhang, H. Gu, and Y. Yang, A High Performance Optical Network on Chip Based on Clos Topology, in *Proceedings of the IEEE International Conf. Future Computer and Communication (ICFCC),* Vol. 2, 2010, pp. 63-68.

[11]. Somayyeh Koohi, Meisam Abdollahi, Shaahin Hessabi, All-Optical Wavelength-Routed NoC based on a Novel Hierarchical Topology, in *Proceedings of the IEEE/ACM International Symposium on Network on Chip,* May 2011, pp. 97-104.

[12]. B. A. Floyd, C. Hung, and K. K. O., Intra-chip wireless interconnect for clock distribution implemented with integrated antennas, receivers, and transmitters, *IEEE Journal of Solid-State Circuits,* Vol. 37, No. 5, May 2002, pp. 543–552.

[13]. Kuan-Neng Chen, Mauro J. Kobrinsky, Brandon C. Barnett et al., Comparisons of Conventional, 3-D, Optical, and RF Interconnects for On-Chip Clock Distribution, *IEEE Transactions on Electron Devices,* Vol. 51, No. 2, February 2004, pp. 233-239.

[14]. Yi Wang, Dan Zhao, The Design and Synthesis of A Synchronous and Distributed MAC Protocol for Wireless Network-on-Chip, in *Proceedings of the IEEE/ACM International Conference on Computer-Aided Design (ICCAD),* November 2007, pp. 612-617.

[15]. D. Zhao, Y. Wang, SD-MAC: Design and synthesis of a hardwareefficient collision-free qos-aware mac protocol for wireless network-onchip, *IEEE Transactions on Computers,* Vol. 57, No. 9, 2008, pp. 1230–1245.

[16]. Dan Zhao, Yi Wang, MTNet Design of a Wireless Test Framework for Heterogeneous Nanometer Systems-on-Chip, *IEEE Transactions on Very Large Scale Integration (VLSI) Systems*, Vol. 16, No. 8, August 2008, pp. 1046-1057.

[17]. R. Wu, Y. Wang, and D. Zhao., A low-cost deadlock-free design of minimal-table rerouted xy-routing for irregular wireless NoCs, in *Proceedings of the 4th ACM/IEEE International Symposium on Networks-on-Chip,* 2010, pp. 199–206.

[18]. Suk-Bok Lee, Saiwang Tam, Loannis Pefkianakis et al., A scalable micro wireless interconnect structure for CMPs, *ACM Mobicom*, September 2009, pp. 217-228.

[19]. D. Zhao, Y. Wang, J. Li, and T. Kikkawa, Design of Multi-Channel Wireless NoC to Improve On-Chip Communication Capacity, in *Proceedings of the 5th IEEE/ACM International Symposium on Networks on Chip (NoCS),* May 2011, pp. 177-184.

[20]. P. P. Pande, A. Ganguly, K. Chang, and C. Teuscher., Hybrid wireless network on chip: A new paradigm in multi-core design, in *Proceedings of the International Workshop on Network on Chip Architectures (NoCArc),* December 2009, pp. 71-76.

[21]. S. Deb, A. Ganguly, K. Chang, P. P. Pande, B. Belzer, and D. Heo, Enhancing Performance of Network-on-Chip Architectures with Millimeter-Wave Wireless Interconnects, in *Proceedings of the IEEE international Conference on ASAP*, 2010, pp. 73-80.

[22]. W. Chifeng, H. Wen-Hsiang, and N. Bagherzadeh, A Wireless Network-on-Chip Design for Multicore Platforms, in *Proceedings of the 19th Euromicro International Conf. Parallel, Distributed and Network-Based Processing (PDP),* February 2011, pp. 409-416.

[23]. A. Ganguly, K. Chang, S. Deb, P. P. Pande, B. Belzer, and C. Teuscher, Scalable Hybrid Wireless Network-on-Chip Architectures for Multicore Systems, *IEEE Transactions on Computer,* Vol. 60, No. 10, October 2011, pp. 1485-1502.

[24]. Wen-Hsiang Hu, Chifeng Wang, Nader Bagherzadeh., Design and Analysis of a Mesh-based Wireless Network-on-Chip, in *Proceedings of the Euromicro International Conference on Parallel, Distributed and Network-based Processing,* February 2012, pp. 483-490.

[25]. Sujay Deb, Kevin Chang, Amlan Ganguly et al., Design of an Efficient NoC Architecture using Millimeter-Wave Wireless Links, in *Proceedings of the IEEE International Symposium on Quality Electronic Design (ISQED),* March 2012, pp. 165-172.

[26]. Sujay Deb, Amlan Ganguly, Partha Pratim Pande et al., Wireless NoC as Interconnection Backbone for Multicore Chips: Promises and Challenges, *IEEE Journal on Emerging and Selected Topics in Circuits and Systems,* Vol. 2, No. 2, June 2012, pp. 228-239.

[27]. Philippe Benech, Anna Triantafyllou et al., Design and performance of integrated antennas for wireless intra-chip interconnections, in *Proceedings of the IEEE Conference on Industrial Electronics*, November 2006, pp. 2953-2957.

[28]. Y. P. Zhang, Bit-Error-Rate Performance of Intra-Chip Wireless Interconnect Systems, *IEEE Communications Letters,* Vol. 8, No. 1, January 2004, pp. 39-41.

[29]. Yue Ping Zhang, Zhi Ming Chen, Mei Sun., Propagation Mechanisms of Radio Waves Over Intra-Chip Channels With Integrated Antennas: Frequency-Domain Measurements and Time-Domain Analysis, *IEEE Transactions on Antenna and Propagation*, Vol. 55, No. 10, October 2007, pp. 2900-2906.

[30]. Mei Sun, Yue Ping Zhang, Guo Xin Zheng et al., Performance of Intra-Chip Wireless Interconnect Using On-Chip Antennas and UWB Radios, *IEEE Transactions on Antennas and Propagation,* Vol. 57, No. 9, September 2009, pp. 2756-2762.

[31]. M. Bialkowski, A. Abbosh., Wireless intrachip-interchip interconnections utilising tapered slot antennas for ultra-large-scale integration technology, IET Microw, *Antennas Propagation*, Vol. 4, No. 10, October 2010, pp. 1665-1671.

[32]. He Xiao Wei, Zhang Min Xuan, Li Jin Wen, Characteristics of on-chip dipole antenna using diamond for intra-chip wireless interconnect*, Science China Technological Sciences,* Vol. 54, No. 4, April 2011, pp. 1035-1043.

[33]. K. Kempa et al., Carbon Nanotubes as Optical Antennae, *Advanced Materials*, Vol. 19, 2007, pp. 421-426.

[34]. Alireza Nojeh, Andre Ivanov, Wireless Interconnect and the Potential for Carbon Nanotubes, *IEEE Design and Test of Computers,* Vol. 27, No. 4, August 2010, pp. 44-53.

[35]. Guo X L., CMOS intra-chip wireless clock distribution, PhD Thesis, *University of Florida*, 2005, 34–36.

[36]. Fu Wei, Ma Jiangguo., Improving the accuracy of two-ray model at 60 GHz for Line-of-sight Wireless Desktop Channel, *Microwave and Optical Technology Letters,* Vol. 51, No. 4, April 2009, pp. 907-910.

---